

OPTICAL AFTERGLOWS OF SHORT GAMMA-RAY BURSTS AND GRB 040924

Y. Z. FAN^{1,2,3}, BING ZHANG¹, SHIHO KOBAYASHI^{4,5} AND PETER MÉSZÁROS^{4,5}

¹ Dept. of Physics, University of Nevada, Las Vegas, NV 89154, USA.

² Purple Mountain Observatory, Chinese Academy of Science, Nanjing 210008, China.

³ National Astronomical Observatories, Chinese Academy of Sciences, Beijing, 100012, China.

⁴ Dept. of Astronomy and Astrophysics, Pennsylvania State University, 525 Davey Laboratory, University Park, PA 16802, USA.

⁵ Dept. of Physics, Pennsylvania State University, 104 Davey Laboratory, University Park, PA 16802, USA.

Accepted for publication in ApJ

ABSTRACT

Short-duration Gamma-ray bursts (GRBs) (≤ 2 s) have remained a mystery due to the lack of afterglow detection until recently. The models to interpret short GRBs invoke distinct progenitor scenarios. Here we present a generic analysis of short GRB afterglows, and calculate the optical lightcurves of short GRBs within the framework of different progenitor models. We show that all these optical afterglows are bright enough to be detected by the Ultraviolet and Optical Telescope (UVOT) on board the *Swift* observatory, and that different models could be distinguished with a well-monitored lightcurve. We also model the afterglow data of the recently discovered short burst GRB 040924. We find that the limited data are consistent with a low medium density environment which is consistent with the pre-concept of the compact-star merger progenitor model, although the models with a collapsar progenitor are not ruled out.

Subject headings: Gamma Rays: bursts—ISM: jets and outflows—radiation mechanisms: nonthermal

1. INTRODUCTION

In the past several years great advances have been made in revealing the nature of Gamma-ray Bursts (GRBs) of relatively long duration, i.e. $T_{90} > 2$ s (e.g. Mészáros 2002; Zhang & Mészáros 2004 for recent reviews). However, another category of GRBs, i.e. those with short durations (i.e. $T_{90} < 2$ s), which comprise about 1/3 of the total GRB population, have remained as mysterious as long GRBs were before 1997. This has been mainly due to the lack of afterglow detections for short GRBs, until very recently.

The leading progenitor model for short GRBs invokes merger of two compact objects (e.g. NS-NS merger or BH-NS merger, Eichler et al. 1989; Paczyński 1991; Narayan et al. 1992; Mészáros & Rees 1992), which has been found suitable to interpret many short GRB properties (Ruffert et al. 1997; Popham et al. 1999; Perna & Belczynski 2002; Rosswog et al. 2003; Aloy et al. 2004). In this scenario, the burst site is expected to have a large offset from the host galaxy due to asymmetric kicks during the birth of NSs (Bloom et al. 1999; but see Belczynski et al. 2002), so that the number density of the external medium in the GRB environment is low, typically $\sim 10^{-2}\text{cm}^{-3}$. Alternatively, with the increasing evidence that long GRB progenitors are collapsars, it has been suggested that short GRBs may also be associated with collapsars, with either a less energetic jet (i.e. short emerging model, Zhang, Woosley & MacFadyen 2003) or a jet composed of many subjects seen by an off-axis observer looking into one or a few subject(s) (subjects model, Yamazaki, Ioka & Nakamura 2004). If this is the case, the environment around the progenitor should be similar to that of long GRBs, which is either a constant density medium (e.g. Panaitescu & Kumar 2002; Yost et al. 2003) with ISM number density $n \sim 1\text{cm}^{-3}$ or a prestellar wind (e.g. Chevalier & Li 2000). Other possibilities for the origin of short GRBs have been proposed

within the cylindrical jet model (Wang et al. 2004) and the Poynting-flux dominated GRB model (Lyutikov & Blandford 2003).

Within the standard afterglow model and adopting a typical compact star merger environment, the forward shock afterglow emission of short GRBs have been calculated by Panaitescu et al. (2001), Perna & Belczynski 2002, and Li et al. (2003). Panaitescu et al. (2001) have shown that the afterglows of short GRBs are faint, and they are likely to be most easily detected in the X-ray band. Li et al. (2003) considered possible e^{\pm} pair loading and evaluated its possible observational signature. In this work, we present a generic treatment of short GRB optical afterglows which differs from the previous ones by including both the forward and the reverse shock emission, a crucial ingredient for characterizing the early afterglow light curve and the spectrum. The model is applied to various progenitor models and sample lightcurves are calculated which are compared against Swift UVOT sensitivity (§2). Lately, a short, soft burst GRB 040924 was located by HETE-2, which led to the discovery of its optical afterglow (Fox & Moon 2004). We also apply the model to fit the afterglow data of this burst (§3).

2. THE AFTERGLOW OF SHORT γ -RAY BURSTS

In the standard afterglow model for a fireball interacting with a constant density medium (e.g., Sari, Piran & Narayan 1998), for the forward shock (FS) emission, the cooling frequency ν_c^f , the typical synchrotron frequency ν_m^f and the maximum spectral flux $F_{\nu,\text{max}}^f$ read

$$\nu_c^f = 4.3 \times 10^{17} \text{Hz} E_{51}^{-1/2} \epsilon_{\text{B},-2}^{-3/2} n_{-2}^{-1} t_d^{-1/2} \left(\frac{2}{1+z} \right), \quad (1)$$

$$\nu_m^f = 3.9 \times 10^{11} \text{Hz} E_{51}^{1/2} \epsilon_{\text{B},-2}^{1/2} \epsilon_e^2 t_d^{-3/2} \left[\frac{13(p-2)}{3(p-1)} \right]^2 \left(\frac{2}{1+z} \right), \quad (2)$$

$$F_{\nu,\text{max}}^f = 8.3 \mu\text{Jy} E_{51}^{1/2} \epsilon_{\text{B},-2}^{1/2} n_{-2}^{1/2} D_{28.34}^{-2} \left(\frac{1+z}{2} \right), \quad (3)$$

where E is the isotropic energy of the outflow, ϵ_e and ϵ_B are the fractions of the shock energy given to the magnetic field and electron at the shock, respectively, n is the number density of the external medium, $p \sim 2.3$ is the power-law distribution index of shocked electrons, D is the luminosity distance, and z is the redshift. Hereafter $t = t_{\text{obs}}/(1+z)$ denotes the observer's time corrected for the cosmological time dilation effect, and t_d is in unit of day. The superscript "f" ("r") represent the forward (reverse) shock emission respectively. Throughout this work, we adopt the convention $Q_x = Q/10^x$ using cgs units. We have normalized the parameters to typical values of short GRBs. The above equations apply to an isotropic fireball, or to a jet with opening angle θ_0 when the bulk Lorentz factor $\gamma > 1/(\sqrt{3}\theta_0)$, so that $\gamma \approx 8.2E_{51}^{1/8}n_{-2}^{-1/8}t_d^{-3/8}$ is satisfied. If sideways expansion is important, for $\gamma \leq 1/(\sqrt{3}\theta_0)$, one has $\gamma = (\sqrt{3}\theta_0)^{-1}(t_d/t_{0,d})^{-1/2}$, $F_{\nu,\text{max}(J_s)}^f = F_{\nu,\text{max}}^f(t_d/t_{0,d})^{-1}$, $\nu_{c(J_s)}^f \approx \nu_c^f(t_{0,d})$ and $\nu_{m(J_s)}^f \approx \nu_m^f(t_{0,d})(t_d/t_{0,d})^{-2}$ (Rhoads 1999; Sari, Piran & Halpern 1999). If sideways expansion is unimportant, equations (1-2) still hold and equation (3) should be replaced by $F_{\nu,\text{max}(J)}^f \approx F_{\nu,\text{max}}^f(t_d/t_{0,d})^{-3/4}$. Here the subscript J (J_s) represents a jet without (with) significant sideways expansion, respectively. During the reverse shock crossing process, the bulk LF of the ejecta is nearly a constant if the reverse shock is non-relativistic (which is the case for short bursts). We have $F_{\nu,\text{max}}^f \propto t^3$, $\nu_c^f \propto t^{-2}$ and ν_m^f is independent on t .

The time when RS crosses the shell can be estimated by $t_x = \max[t_{\text{dec}}, T_{90,\text{obs}}/(1+z)]$ (Kobayashi, Piran & Sari 1999). The typical duration of short bursts is $T_{90,\text{obs}} \sim 0.2\text{s}$, which is much smaller than the deceleration time t_{dec} for the ISM case. We therefore have a typical thin-shell regime. the RS is only mildly-relativistic at the shock crossing time (e.g. Sari & Piran 1999; Kobayashi 2000). The typical deceleration radius is defined as $R_{\text{dec}} \approx 5.6 \times 10^{16}\text{cm} E_{51}^{1/3} n_{-2}^{-1/3} \eta_{2.5}^{-2/3}$ (Rees & Mészáros 1992), where $\eta \sim 300$ is the initial Lorentz factor (LF) of the outflow. At R_{dec} , the LF of the outflow drops to $\gamma_x = \gamma_{\text{dec}} \sim 0.6\eta$, so that $t_{\text{dec}} \approx R_{\text{dec}}/2\gamma_{\text{dec}}^2 c = 30\text{s} E_{51}^{1/3} n_{-2}^{-1/3} \eta_{2.5}^{-8/3}$.

At $t_x = t_{\text{dec}}$, the LF of the decelerated outflow relative to the initial one is $\gamma_{34,x} \approx (\eta/\gamma_x + \gamma_x/\eta)/2 = 1.13$. The typical frequency of the RS emission can be estimated by

$$\nu_m^r(t_x) = \mathcal{R}_B \frac{(\gamma_{34,x} - 1)^2}{(\gamma_x - 1)^2} \nu_m^f(t_x) \propto n^{1/2}, \quad (4)$$

where \mathcal{R}_B is the ratio of the magnetic field in the reverse emission region to that in the FS emission region (Zhang, Kobayashi & Mészáros 2003). Since at least for some bursts (e.g. GRB990123 and GRB021211) the RS emission region seems to be more strongly magnetized (e.g. Fan et al. 2002; Zhang et al. 2003; Kumar & Panaitescu 2003), here we adopt two typical values, i.e. $\mathcal{R}_B = 5$ and 1, in the calculations. There are two possibilities for a magnetized flow (e.g. Fan et al. 2004). The central engine may directly eject magnetized shells. Alternatively, the magnetic fields generated in the internal shock phase may not be dissipated significantly in a short period of time (e.g. Medvedev et al. 2005), and they can

get amplified again in the RS region. This second effect, which has been ignored previously, should also play an important role in calculating the afterglow re-brightening effect in refresh-shocks.

Following Kobayashi & Zhang (2003a) and Zhang et al. (2003), we have

$$\nu_c^r \approx \mathcal{R}_B^{-3} \nu_c^f \propto n^{-1}, \quad (5)$$

$$F_{\nu,\text{max}}^r(t_x) \approx \eta \mathcal{R}_B F_{\nu,\text{max}}^f(t_x) \propto n^{1/2}. \quad (6)$$

Generally, the R-band flux satisfies $F_{\nu_R}(t_x) \approx F_{\nu,\text{max}}^r(t_x)[\nu_R/\nu_m^r(t_x)]^{-(p-1)/2} \propto n^{\frac{p+1}{4}}$. In the thin shell case, the R-band RS flux is $F_{\nu_R}^r \propto t_{\text{obs}}^{2p}$ for $t_{\text{obs}} < (1+z)t_x$, and is $F_{\nu_R}^r \propto t_{\text{obs}}^{-2}$ for $t_{\text{obs}} > (1+z)t_x$ (e.g., Sari & Piran 1999; Kobayashi 2000).

If short GRBs are born in a stellar wind (for the collapse model), for the FS emission, the cooling frequency $\bar{\nu}_c^f$, the typical synchrotron frequency $\bar{\nu}_m^f$ and the maximum spectral flux $\bar{F}_{\nu,\text{max}}^f$ read (Chevalier & Li 2000)

$$\bar{\nu}_c^f = 2 \times 10^{13}\text{Hz} \epsilon_{B,-2}^{-3/2} E_{51}^{1/2} A_*^{-2} \left(\frac{2}{1+z}\right) t_d^{1/2}, \quad (7)$$

$$\bar{\nu}_m^f = 4.5 \times 10^{12}\text{Hz} \epsilon_{e,-0.5}^2 \epsilon_{B,-2}^{1/2} E_{51}^{1/2} \left(\frac{2}{1+z}\right) t_d^{-3/2}, \quad (8)$$

$$\bar{F}_{\nu,\text{max}}^f \approx 3.8\text{mJy} \epsilon_{B,-2}^{1/2} E_{51}^{1/2} A_* D_{28.34}^{-2} \left(\frac{1+z}{2}\right) t_d^{-1/2}, \quad (9)$$

where $A_* = (\dot{M}/10^{-5}M_{\odot}\text{yr}^{-1})(v_w/10^3\text{km s}^{-1})^{-1}$, \dot{M} is the mass loss rate of the progenitor, and v_w is the wind velocity. Here the bar-parameters represent the wind case.

Equations (7-9) apply to an isotropic fireball, or to a jet with opening angle θ_0 when the bulk Lorentz factor $\gamma > 1/\sqrt{3}\theta_0$, so that $\gamma \approx 3.3E_{51}^{1/4}A_*^{-1/4}t_d^{-1/4}$ is satisfied. For $\gamma \leq 1/\sqrt{3}\theta_0$, if sideways expansion is significant, the emission properties is similar to the ISM case (Sari et al. 1999; Chevalier & Li 2000). If sideways expansion is unimportant, equations (7-8) still hold and equation (9) should be replaced by $\bar{F}_{\nu,\text{max}(J)}^f \approx \bar{F}_{\nu,\text{max}}^f(t_d/\bar{t}_{0,d})^{-1/2}$, where $\bar{t}_{0,d}$ is determined by $3.3E_{51}^{1/4}A_*^{-1/4}\bar{t}_{0,d}^{-1/4} = 1/\sqrt{3}\theta_0$.

In the wind case, the RS is usually relativistic (e.g., Chevalier & Li 2000). The resulting $t_x \sim T_{90}$, and the optical emission typically drops as $(t/t_x)^{-3}$ for $t > t_x$ (Kobayashi & Zhang 2003b, Kumar & Panaitescu 2000). For short bursts, the duration when the reverse shock emission dominates is too short for any observational interest. In this work, we do not include the RS emission in the wind models. Below we calculate the typical optical-band lightcurves for short GRBs within different progenitor models.

2.1. Compact star merger model

The afterglows of short GRBs powered by mergers have been investigated by Panaitescu et al. (2001) numerically. Here we re-calculate the optical afterglow lightcurve by also taking into account the RS emission.

The lightcurves for this model are plotted as solid lines in Figure 1. At the deceleration time [$\sim 40(1+z)$ s after the burst trigger], the RS emission reaches its peak,

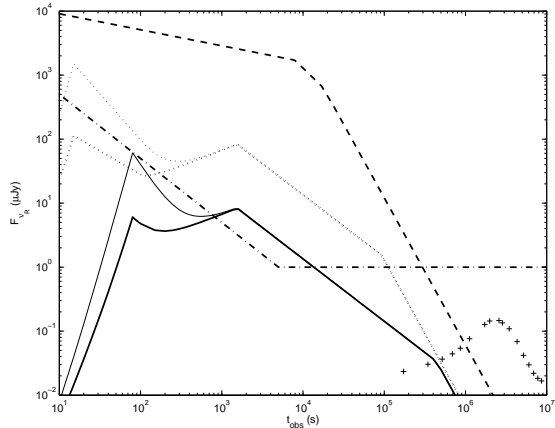


FIG. 1.— The analytical R-band lightcurves of short GRBs in the compact star merger model and the short emerging model. The solid lines, dotted lines and the dashed line represent the compact star merger model in the ISM environment, the short emerging collapsar model in the ISM environment, and the same model in the wind environment, respectively. For the first two models (the ISM models), the reverse shock emission component was calculated for both $\mathcal{R}_B = 5$ (the thin lines) and $\mathcal{R}_B = 1$ (the thick lines). The thick dash-dotted line represents the sensitivity of UVOT. For $t_{\text{obs}} > 5000\text{s}$, the exposure time of UVOT is assumed to be 1000s, while for $t_{\text{obs}} < 5000\text{s}$, it is assumed to be $t_{\text{obs}}/5$. Following parameters are adopted in the calculations: $\eta = 300$, $\epsilon_e = 0.3$, $\epsilon_B = 0.01$, $p = 2.3$, $z = 1$, $D = 2.2 \times 10^{28}\text{cm}$. In both the compact star merger model and the short emerging model ISM model, it is assumed that the outflow is jet-like with an opening angle $\simeq 0.1$ and an isotropic energy $\simeq 10^{51}\text{ergs}$. The ISM number density is taken as 0.01cm^{-3} and 1cm^{-3} , respectively. For the short-emerging wind model, the density is taken as $n = 3 \times 10^{35} R^{-2}\text{cm}^{-3}$. For indicative purpose, we also plotted a template 1998bw-like supernova R-band lightcurve at redshift $z = 1$ (the line of plus signs).

and the R band brightness is 20 mag for $\mathcal{R}_B = 5$ (thin solid line) and $z = 1$. Swift UVOT has a sensitivity of 24 mag during 1000s exposure time. Scaling down with time, the sensitivity should be 19 mag for 10s exposure. Unless the event is much closer or R_B is larger, the RS emission is likely to be below the UVOT sensitivity. The FS emission is quite similar to the numerical calculation of Panaitescu, et al. (2001). Because of a lower n and a smaller E , the R-band afterglow is much dimmer than that of typical long GRBs, but it is still detectable by the UVOT for at least a few hours. In the compact star merger scenario, the collimation of the outflow is quite uncertain. Here we adopt $\theta_0 \sim 0.1$ as suggested in numerical simulations (e.g. Aloy et al. 2004). As shown in Figure 1, the lightcurve break occurs too late to be detected with the current telescope sensitivity.

2.2. Short emerging model

In the “short emerging model” (Zhang, Woosley & MacFadyen 2003), physical parameters (including the medium density n and the jet opening angle $\theta_0 \simeq 0.1$) are generally similar to the familiar long GRBs, except that the isotropic energy is smaller. This model has received support from a recent comparison study of the spectral properties of long and short GRBs (Ghirlanda, Ghisellini & Celotti 2004). The R-band lightcurves of this model are plotted as dotted lines in Fig.1 for ISM case, where the thin and thick lines are for $\mathcal{R}_B = 5$ and $\mathcal{R}_B = 1$, respectively. Compared with the compact star merger model, thanks to a larger n ($F_{\nu, \text{max}}^f \propto n^{1/2}$ and

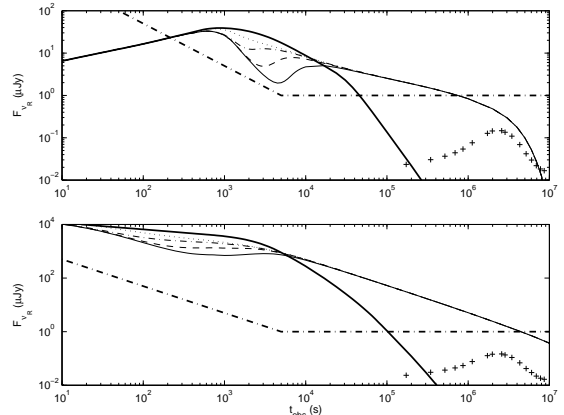


FIG. 2.— The R-band lightcurves of short GRBs for the subjet model. The typical lightcurve for the short emerging model is also plotted for comparison. The upper panel is for the ISM case ($n = 1\text{cm}^{-3}$), and the lower one is for the wind case ($n = 3.0 \times 10^{35} R^{-2}\text{cm}^{-3}$). The thin lines are for the subjet model. The dotted, dash-dotted line, dashed line and solid lines represent $\Delta\theta = 0, 0.01, 0.02, 0.03$ respectively. For clarity, only the forward shock emission is taken into account. Following parameters are adopted. For the on-beam subjet, the jet opening angle is $\theta_{\text{sub}} = 0.02$, and the isotropic energy is 10^{51}ergs . For the Gaussian jet, the typical Gaussian angle is $\theta_c = 0.08$, the maximum angle is 0.3, and angle-dependent energy per solid angle reads $\epsilon = (10^{53}/4\pi) \exp(-\theta^2/2\theta_c^2)$. The line-of-sight angle is $\theta_v = 0.26$ from the jet axis. The thick solid line is for the short emerging model calculated with the same code to calculate the subjet model. The thick dash-dotted line represents the sensitivity of UVOT. Other parameters such as η , ϵ_e , ϵ_B , p and z are the same as those adopted to calculate Fig. 1. The supernova bump is also illustrated.

$\nu_m^f \propto n^0$ for $\gamma \geq (\sqrt{3}\theta_0)^{-1}$), the RS peak flux is above the UVOT threshold, if \mathcal{R}_B is somewhat larger than unity. The RS emission peaks earlier (due to a smaller deceleration radius) so that the RS peak may be missed if it is shorter than the slewing time. In any case, the t_{obs}^{-2} decaying component can be detected for $\mathcal{R}_B = 5$ for a $z = 1$ burst. In the wind case, for standard parameters (e.g. $n = 3 \times 10^{35} R^{-2}\text{cm}^{-3}$ or $A_* = 1$), the resulting R-band lightcurve is very bright (see the thick dashed line plotted in Fig. 1), thanks to a relative denser medium at $R < 5.5 \times 10^{17}\text{cm}$.

2.3. Subjet model

In the subjet model (Yamazaki, Ioka & Nakamura 2004), GRBs are conjectured as being powered by many intrinsically similar subjets, and the number of the subjets are distributed with angle as a Gaussian function (Zhang & Mészáros 2002), i.e. $n \propto \exp[-(\theta/\sqrt{2}\theta_c)^2]$, with the typical Gaussian angle $\theta_c \simeq 0.1$ (Zhang et al. 2004). If an observer is far away from the jet axis and by chance is on the beam of one subjet, one detects a short burst. The global afterglow emission of this model could be then approximated by that of a Gaussian structured jet superimposed on a uniform subjet. Here we consider two emission components, one on-beam uniform less-energetic subjet with an opening angle $\theta_{\text{sub}} \approx 0.02$, and another stronger and wider Gaussian structured jet with typical Gaussian angle $\theta_c = 0.08$ with the line-of-sight angle $\theta_v \simeq 3\theta_c$ off-axis. Since the Gaussian angular distribution is only of statistical sense in the subjet model (Yamazaki et al. 2004), around the subjet there could be

a “void” where the emissivity is below the Gaussian jet model in order to counterbalance the emissivity excess at the subjet. Here we approximate this effect by adopting an annular void region of width $\Delta\theta$ around the subjet axis (i.e. the emissivity is zero in the range from θ_{sub} to $\theta_{\text{sub}} + \Delta\theta$). In view of the uncertainties, we calculate the lightcurves for $\Delta\theta = 0, 0.01, 0.02, 0.03$, respectively. Following Yamazaki et al. (2004) we include a maximum Gaussian jet angle $\theta_j = 0.3$ in the calculation.

The afterglow lightcurves of structured jets have been modeled by many authors (e.g., Wei & Jin 2003; Kumar & Granot 2003; Granot & Kumar 2003; Panaitescu & Kumar 2003; Salmonson 2003; Rossi et al. 2004). Here we take the simple method proposed by Wei & Jin (2003), in which the sideways expansion of the jet is ignored (see Kumar & Granot 2003 for justification) but the “equal arriving surface” effect is taken into account. The jet evolution is quantified by $\gamma = (3\epsilon/n)^{1/2}(m_p c^2)^{-1/2}[ct/(1 - \mu + 1/16\gamma^2)]^{-3/2}$ for the ISM case, and by $\gamma = (\epsilon/3 \times 10^{35} A_*)^{1/2}(m_p c^2)^{-1/2}[ct/(1 - \mu + 1/8\gamma^2)]^{-1/2}$ for the wind case¹. Here $\epsilon = (10^{53}/4\pi)\exp(-\theta^2/2\theta_c^2)$ is the energy per unit solid angle of the structured jet, $\mu = \cos\Theta$, Θ is the angle between the moving direction of an emitting unit and the line of sight. The isotropic energy of the on-beam subjet is taken as 10^{51} ergs. The sideways expansion of the on-beam subjet is also ignored. At any emission unit, the standard broken power-law synchrotron spectrum (e.g. Sari et al. 1998) is adopted with $\delta F_{\nu, \text{max}}^f \approx 3\sqrt{3}\Phi_p(1+z)\delta N_e m_e c^2 \sigma_T B / \{32\pi^2 e D^2 [\gamma(1 - \beta\mu)]^3\}$ (Wijers & Galama 1999), where Φ_p is a function of p (for $p \simeq 2.3$, $\Phi_p \simeq 0.60$), B is the magnetic field generated at the shock front. In the ISM case, we take the total number of electrons swept in the solid angle $d\Omega$ as $\delta N_e = d\Omega R^3 n/3$, where R is the radius of the FS front. In the wind case, $\delta N_e = 3.0 \times 10^{35} R d\Omega$ is adopted.

The model lightcurves for the subjet model are plotted separately in Fig.2. The upper panel is the ISM case and the lower panel is the wind case. For a comparison, the lightcurve of short emerging model is also plotted in each model (the thick solid line), which is similar to the analytical result presented in Figure 1. For the subjet model, at the early times, the R-band emission is dominated by the on-beam subjet. As the subjet is decelerated so that the Lorentz factor is of order θ_{sub} , a very early jet break appears (see Fig 2 for detail). On the other hand, the energetic Gaussian core component contributes to the emission steadily, becomes progressively important at later times, and dominates the afterglow level after thousands of seconds. Because of the progressively important core contribution, the afterglow decay in the subjet model is much slower than that in the short merging model. Notice that the subjet model could be different from the usual Gaussian jet model in which the angular energy distribution is smooth (e.g. Kumar & Granot 2003; Rossi et al. 2004). The possible existence of the void around the subjet may lead to an afterglow bump (see Figure 2). In fact, if $\Delta\theta$ is 0.1 or larger, the whole jet can be approximated as two distinct components, i.e. a weak on-beam sub-jet and an off-beam but

¹ In the wind case, if we define $X \equiv \epsilon/(3 \times 10^{35} A_* m_p c^3 t)$, one has $\gamma = [X(1 - \mu) + \sqrt{X^2(1 - \mu)^2 + 4X}]/2$, and the solutions could be coasted into a simple form.

more energetic uniform core since the result is insensitive to the detailed structure in the core. The bump can be then understood in terms of the off-beam orphan afterglow models (e.g. Granot et al. 2002). In our calculations the initial Lorentz factor across the whole jet is assumed to be independent on the angle (Yamazaki et al. 2004).

For both the short-emerging model and the subjet model, one may expect a Type Ib/c supernova component (usually a red bump) showing up a few weeks after the burst trigger, as has been detected in some long GRBs. For illustrative purpose, we plot in Fig.1 and Fig. 2 a template 1998bw-like supernova lightcurve at $z = 1$. The afterglows of short bursts are typically fainter than those of the long ones, so the supernova signature should be easily distinguishable, especially for the short emerging model. For the subjet model, the contamination of the core component may make the identification of the SN component more difficult. In any case, if a flattening or bump is detected within weeks for a short GRB afterglow, it would argue against the compact star merger model.

3. GRB 040924

GRB 040924 triggered the High Energy Transient Explorer 2 (HETE-2) on 2004 September 24 at 11:52:11 UT (Fenimore et al. 2004). The burst lasted $T_{50} \sim 1.2$ s, and the energy fluence was $\mathcal{F}_\gamma \sim 7.7 \times 10^{-6}$ ergs cm^{-2} (Fenimore et al. 2004; Golenetskii et al. 2004). The ratio of the fluence in the 7-30 keV band and in the 30-400 keV band is about 0.6, so that the burst is classified as an X-ray rich GRB. The burst redshift was identified as $z = 0.859$ (Wiersema et al. 2004). The prompt localization of GRB 040924 by HETE-2 allowed follow-up observations of its afterglow at early times (Fox & Moon 2004; Li et al. 2004). Fox (2004) detected an optical transient ~ 16 minutes after the trigger at the level of $m_R \simeq 18.0$ mag. At the same position, Li et al. (2004) detected an optical transient ~ 26 and ~ 63 minutes after the trigger at the level of $m_R \simeq 18.3$ mag and 19.2mag, respectively. Later detections in K-band and R-band have been reported by many groups (Terada & Akiyama 2004; Terada, Akiyama & Kawai 2004; Hu et al. 2004; Fynbo et al. 2004; Khamitov et al. 2004a, b, c). The radio observation provides an upper limit of 0.12mJy at ~ 15 hours after the burst (van der Horst 2004). Below we will compare the available data with the models, aiming at constraining the burst environment and the possible progenitor.

3.1. ISM case

The constraint $F_{\nu, \text{max}}^f \geq 250 \mu\text{Jy}$ results in $f_\gamma \mathcal{F}_{\gamma, -5.1}^{1/2} \epsilon_{B, -2}^{1/2} n_{-2}^{1/2} \geq 1.3$, where $f_\gamma \geq 1$ is the ratio of the afterglow energy to the γ -ray energy. With $z = 0.859$ and taking $f_\gamma = 2$, we can estimate $E \simeq 3 \times 10^{52}$ ergs within the standard cosmology. At the time $t_R \leq 945$ s, the typical frequency of the FS emission crosses the observer frequency (R-band, $\nu_{\text{obs}} = 4.6 \times 10^{14}$ Hz). This results in $0.12 [\frac{3(p-1)}{13(p-2)}]^2 (t_R/945 \text{ s})^{3/2} = E_{52.5}^{1/2} \epsilon_{B, -2}^{1/2} \epsilon_{e, -0.5}^2 (1+z)^{1/2}$. We then have the following constraints

$$\epsilon_e \leq 0.1 [\frac{3(p-1)}{13(p-2)}] (\frac{t_R}{945})^{3/4} E_{52.5}^{-1/4} (f_\gamma/2)^{1/2} \mathcal{F}_{\gamma, -5.1}^{1/2} n_{-2}^{1/4},$$

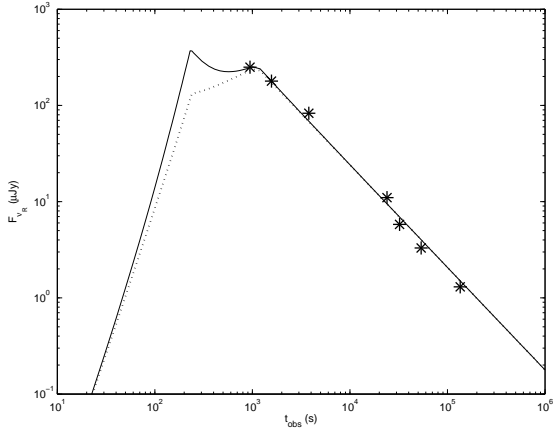


FIG. 3.— Modelling the R-band afterglow data of GRB 040924. The identified burst redshift is $z = 0.859$, and the total fluence is $\mathcal{F}_\gamma = 7.7 \times 10^{-6}$ ergs (Wiersema et al. 2004). This gives $E_\gamma \simeq 1.5 \times 10^{52}$ erg assuming isotropic emission. The data (marked by asterisk) are taken from Fox (2004), Li et al. (2004), Hu et al. (2004) and Khamitov et al. (2004a, b, c). The solid line and dotted line are the theoretical afterglow lightcurves of a slow cooling fireball (or a jet with wide opening angle) expanding into a low density ISM. The parameters are $E = 3 \times 10^{52}$ ergs, $f_\gamma = 2$, $\epsilon_e = 0.1$, $\epsilon_B = 0.004$, $n = 0.01 \text{ cm}^{-3}$ and $p = 2.42$. The solid and dotted lines are for $\mathcal{R}_B = 3$ and $\mathcal{R}_B = 1$, respectively.

$$\epsilon_B \geq 4 \times 10^{-3} (f_\gamma/2)^{-2} \mathcal{F}_{\gamma, -5.1}^{-2} n_{-2}^{-1}.$$

The observed temporal decay slope is $\alpha_{\text{obs}} \simeq -1.07$, which gives $p = 2.42$ in the standard afterglow model. The resulting spectral index $\beta \simeq -0.71$ matches the observation $\beta_{\text{obs}} = 0.61 \pm 0.08$ (Silvey et al. 2004). Assuming $t_R \approx 945$ s and $F_{\nu, \text{max}}^f = 250 \mu\text{Jy}$ and $n = 0.01 \text{ cm}^{-3}$, one gets $\epsilon_e \approx 0.1$ and $\epsilon_B \approx 0.004$. The values of the parameters ϵ_e and ϵ_B fall into the regime inferred from afterglow modeling of long bursts (Panaitescu & Kumar 2002; Yost et al. 2003). We note that if we take $n \sim 1 \text{ cm}^{-3}$, $\epsilon_B \sim 10^{-5}$ is obtained. If the shock parameters are more or less universal, our modeling suggests that a low density ISM model is favored, which is consistent with the pre-concept of the merger model. In Fig. 3, we use our model lightcurves to fit the data.

With parameters derived, ν_c^f is above the optical energy band in all the observer time, which is consistent with the observation (Silvey et al. 2004).

3.2. Wind case

In the wind case, for $\beta_{\text{obs}} \simeq 0.61 \pm 0.08$. With the temporal index $\alpha_{\text{obs}} \simeq -1.07$, $\bar{\nu}_m^f < \nu_{\text{obs}} < \bar{\nu}_c^f$ should be satisfied (e.g. Chevalier & Li 2000; see also the Tab. 1 of Zhang & Mészáros 2004 for a summary).

At 945s, the constraints of $\bar{\nu}_c^f > \nu_{\text{obs}}$, $\bar{\nu}_m^f \leq \nu_{\text{obs}}$ and $(\bar{\nu}_m^f/\nu_{\text{obs}})^{(p-1)/2} \bar{F}_{\nu, \text{max}} = 250 \mu\text{Jy}$ yield

$$A_* < 0.14 (f_\gamma/2)^{1/4} \epsilon_{B, -2}^{-3/4}, \quad (10)$$

$$\epsilon_{e, -0.5} = 0.09 g^{1/2} (f_\gamma/2)^{-1/4} \epsilon_{B, -2}^{-1/4}, \quad (11)$$

$$A_* = 5.9 \times 10^{-4} g^{-(p-1)/2} \epsilon_{B, -2}^{-1/2} (f_\gamma/2)^{-1/2}. \quad (12)$$

By taking $\epsilon_B \sim 10^{-3}$ and $f_\gamma = 2$, we have $\epsilon_e \sim 0.05 g^{1/2}$ and $A_* \sim 1.8 \times 10^{-3} g^{-(p-1)} < 0.8$, where we have defined

$g = \bar{\nu}_m^f/\nu_{\text{obs}}$. Therefore, unless ϵ_e is much smaller than the typical value 0.1, we get a very weak stellar wind $A_* \sim 10^{-3}$. A second problem of the wind model comes from the temporal index. For $\beta_{\text{obs}} \simeq 0.61$ (Silvey et al. 2004), we have $p \simeq 2.22$, which in turn results in $\alpha \simeq -1.4$. This is significantly steeper than α_{obs} . We thus suggest that the wind model is less favored.

In summary, we suggest that the circumburst medium is preferably a constant density ISM. If we believe that the shock parameters does not vary significantly among bursts, the inferred n is significantly lower than that of the typical ISM, which coincides with the pre-concept of the compact objects merger model. No definite jet break is detected, so we do not know the geometrically corrected γ -ray energy. If GRB 040924 is indeed powered by a merger event, no associated Ib/Ic supernova signature (typically a red lightcurve bump with flux $1 \mu\text{Jy}$ at $z \sim 1$) is expected in a few weeks after the burst. The negative detection of the supernova signature at the time when this work is completed (two months after the burst trigger) is also consistent with the compact star merger model.

4. SUMMARY & DISCUSSION

We have modeled the typical optical afterglow lightcurves for short bursts within the context of the leading progenitor models. Both the forward and reverse shock emission components are considered. With typical parameters, the early afterglows should be detectable by the Swift UVOT, and a well-monitored lightcurve can help to identify the progenitors of short bursts.

The optical afterglow data collected so far for the recent bright short burst GRB 040924 can be modeled well with an isotropic fireball expanding into a low density medium with $n \sim 10^{-2} \text{ cm}^{-3}$. The wind model is found to be less favored. The resulting parameters are consistent with the pre-concept of the compact star merger model. Other models such as a collapsar progenitor with low-density environment, however, cannot be ruled out at this stage. In principle, if GRB 040924 came from a collapsar, a lightcurve flattening is expected within weeks resulting from either the supernova component or the central core component for the subject model. The non-detection of such a feature so far presents a further constraint on the collapsar model.

GRB 040924 is a relatively soft event. It may not be a good representative of the traditional short-hard bursts. Swift will locate more short-hard bursts, and our analysis could be directly utilized to discuss their nature.

YZF thanks D. M. Wei for helpful comments. We also thank the anonymous referee for helpful suggestions. This work is supported by NASA NNG04GD51G (for BZ), Eberly Research Funds of Penn State and by the Center for Gravitational Wave Physics under grants PHY-01-14375 (for SK), NASA AST 0098416 and NASA NAG5-13286 (for PM), and a NASA Swift GI (Cycle 1) program (for BZ, SK and PM).

REFERENCES

- Aloy, M. A., Janka, H. T., & Müller, E. 2004, *A&A*, submitted (astro-ph/0408291)
- Belczynski, K., Bulik, T., & Kalogera, V. 2002, 571, L147
- Bloom, J. S., Sigurdsson, S., & Pols, O. R. 1999, *MNRAS*, 305, 763
- Eichler, D., Livio, M., Piran, T., & Schramm, D. N. 1989, *Nature*, 340, 126
- Chevalier, R. A., & Li, Z. Y. 2000, *ApJ*, 536, 195
- Fan, Y. Z., Dai, Z. G., Huang, Y. F., & Lu, T. 2002, *Chin. J. Astron. Astrophys.* 2, 449
- Fan, Y. Z., Wei, D. M., & Wang, C. F. 2004, *A&A*, 424, 477
- Fenimore, E. E., Ricker, G., Atteia, J-L., Kawai, N., Lamb, D., & Woosley, S. 2004, *GCN Circ.* 2735 (<http://gcn.gsfc.nasa.gov/gcn/gcn3/2735.gcn3>)
- Fox, D. B. 2004, *GCN Circ.* 2741 (<http://gcn.gsfc.nasa.gov/gcn/gcn3/2741.gcn3>)
- Fox, D. B., & Moon, D. S. 2004, *GCN Circ.* 2734 (<http://gcn.gsfc.nasa.gov/gcn/gcn3/2734.gcn3>)
- Fynbo, J. P. U., Hornstrup, A., Hjorth, J., Jensen, B. L., & Andersen, M. I. 2004, *GCN Circ.* 2747 (<http://gcn.gsfc.nasa.gov/gcn/gcn3/2747.gcn3>)
- Ghirlanda, G., Ghisellini, G., & Celotti, A. 2004, *A&A*, 422, L55
- Golenetskii, S., Aptekar, R., Mazets, E., Pal'shin, V., & Frederiks, D. 2004, *GCN Circ.* 2754 (<http://gcn.gsfc.nasa.gov/gcn/gcn3/2754.gcn3>)
- Granot, J., & Kumar, P. 2003, *ApJ*, 591, 1086
- Granot, J., Panaitescu, A., Kumar, P., & Woosley, S. E. 2002, *ApJ*, 570, L61
- Hu, J. H., et al. 2004, *GCN Circ.* 2744 (<http://gcn.gsfc.nasa.gov/gcn/gcn3/2744.gcn3>)
- Khamitov, I. et al. 2004a, *GCN Circ.* 2740 (<http://gcn.gsfc.nasa.gov/gcn/gcn3/2740.gcn3>)
- . 2004b, *GCN Circ.* 2749 (<http://gcn.gsfc.nasa.gov/gcn/gcn3/2749.gcn3>)
- . 2004c, *GCN Circ.* 2752 (<http://gcn.gsfc.nasa.gov/gcn/gcn3/2752.gcn3>)
- Kobayashi, S. 2000, *ApJ*, 545, 807
- Kobayashi, S., Piran, T. & Sari, R. 1999, *ApJ*, 513, 669
- Kobayashi, S., & Zhang, B. 2003a, *ApJ*, 582, L75
- . 2003b, *ApJ*, 597, 455
- Kumar, P. & Granot, J. 2003, *ApJ*, 591, 1075
- Kumar, P. & Panaitescu, A. 2000, *ApJ*, 541, L51
- . 2003, *MNRAS*, 346, 905
- Li, W., Filippenko, R., Chornock, R., & Jha, S. 2004, *GCN Circ.* 2748 (<http://gcn.gsfc.nasa.gov/gcn/gcn3/2748.gcn3>)
- Li, Z., Dai, Z. G., & Lu, T. 2003, *MNRAS*, 345, 1236
- Lyutikov, M., & Blandford, R. 2003 (astro-ph/0312347)
- Medvedev, M. V., et al. 2005, *ApJ*, 618, L75
- Mészáros, P. 2002, *ARA&A*, 40, 137
- Mészáros, P., & Rees, M. J. 1992, *ApJ*, 397, 570
- Narayan, R., Paczyński, B., & Piran, T. 1992, *ApJ*, 395, L83
- Paczynski, B. 1991, *AcA*, 41, 257
- Panaitescu, A., & Kumar, P. 2002, *ApJ*, 571, 779
- . 2003, *ApJ*, 592, 390
- Panaitescu, A., Kumar, P., & Narayan, P. 2001, *ApJ*, 561, L171
- Perna, R., & Belczynski, K. 2002, *ApJ*, 570, 252
- Popham, R., Woosley, S. E., & Fryer, C. 1999, *ApJ*, 518, 356
- Rees, M. J., & Mészáros, P. 1992, *MNRAS*, 258, 41
- Rhoads, J. E. 1999, *ApJ*, 525, 737
- Rossi, E., Lazzati, D., Salmonson, J. D., & Ghisellini, G. 2004, *MNRAS*, 354, 86
- Rosswog, S., Ramirez-Ruiz, E., & Davies, M. B. 2003, *MNRAS*, 345, 1077
- Ruffert, M., et al. 1997, *A&A*, 319, 122
- Salmonson, J. D. 2003, *ApJ*, 592, 1002
- Sari, R., & Piran, T. 1999, *ApJ*, 517, L109
- Sari, R., Piran, T., & Halpern, J. P. 1999, *ApJ*, 519, L17
- Sari, R., Piran, T., & Narayan, R. 1998, *ApJ*, 497, L17
- Silvey, J. et al. 2004, *GCN Circ.* 2833 (<http://gcn.gsfc.nasa.gov/gcn/gcn3/2833.gcn3>)
- Terada, H., & Akiyama, M. 2004, *GCN Circ.* 2742 (<http://gcn.gsfc.nasa.gov/gcn/gcn3/2742.gcn3>)
- Terada, H., Akiyama, M., & Kawai, N. 2004, *GCN Circ.* 2750 (<http://gcn.gsfc.nasa.gov/gcn/gcn3/2750.gcn3>)
- Wang, X. Y., Cheng, K. S., & Tam, P. H. 2004, *ApJ*, in press
- Wei, D. M., & Jin, Z. P. 2003, *A&A*, 400, 415
- Wijers, R. A. M. J., & Galama, T. J. 1999, *ApJ*, 523, 177
- Wiersema, K., Starling, R. L. C., Rol, E., Vreeswijk, P., Wijers, R. A. M. J. 2004, *GCN Circ.* 2800 (<http://gcn.gsfc.nasa.gov/gcn/gcn3/2800.gcn3>)
- van der Horst, A. J., Rol, E., & Wijers, R. A. M. J. 2004, *GCN Circ.* 2746 (<http://gcn.gsfc.nasa.gov/gcn/gcn3/2746.gcn3>)
- Yamazaki, R., Ioka, K., & Nakamura, T. 2004, *ApJ*, 607, L103
- Yost, S., Harrison, F. A., Sari, R., & Frail, D. A. 2003, *ApJ*, 597, 459
- Zhang, B., Dai, X., Lloyd-Ronning, N.M. & Mészáros, P. 2004, *ApJ*, 601, L119
- Zhang, B., Kobayashi, S., & Mészáros, P. 2003, *ApJ*, 595, 950
- Zhang, B., & Mészáros, P. 2002, *ApJ*, 571, 876
- . 2004, *Int. J. Mod. Phys. A.*, 19, 2385
- Zhang, W., Woosley, S. E., & MacFadyen, A. I. 2003, *ApJ*, 586, 356